Perception of complex Glass patterns through spatial summation across unique frames

Published Version:
Roccato, M., Campana, G., Vicovaro, M., Donato, R., Pavan, A. (2024). Perception of complex Glass patterns through spatial summation across unique frames. VISION RESEARCH, 216, 1-9 [10.1016/j.visres.2024.108364].

Availability:
This version is available at: https://hdl.handle.net/11585/959505 since: 2024-02-23

Published:
DOI: http://doi.org/10.1016/j.visres.2024.108364

Perception of complex Glass patterns through spatial summation across unique frames

Marco Roccato[1,2*,†], Gianluca Campana[1,2], Michele Vicovaro[1], Rita Donato[1,3,4], Andrea Pavan[5,†]

[1] Dipartimento di Psicologia Generale, University of Padova, Via Venezia 8, 35131, Padova, Italy

[2] Human Inspired Technology Research Centre, University of Padova, Via Luzzati 4, 35121 Padova, Italy

[3]Proaction Laboratory, University of Coimbra, Faculty of Psychology and Educational Sciences, Colégio de Jesus, Rua Inácio Duarte 65, 3000-481 Coimbra, Portugal.

[4]CINEICC, University of Coimbra, Faculty of Psychology and Educational Sciences, Rua Colégio Novo, 3000-115 Coimbra, Portugal

[5]Department of Psychology, University of Bologna, Viale Berti Pichat 5, 40127 Bologna, Italy.

***Corresponding author**

Marco Roccato

Dipartimento di Psicologia Generale

University of Padova

Via Venezia 8, 35131, Padova, Italy

Email: marco.roccato@phd.unipd.it

[†] These authors contributed equally to this work

Abstract

When processing visual information from the surroundings, human vision depends on the constant integration of form and motion cues. Dynamic Glass patterns (GPs) may be used to study how such visual integration occurs in the human visual system. Dynamic GPs are visual stimuli composed of two or more unique frames consisting of different configurations of dot pairs, called dipoles, presented in rapid succession. Previous psychophysical studies showed that the discrimination of translational and circular dynamic GPs is influenced by both the number of unique frames and the pattern update rate. In this study, we manipulated these two variables to assess their influence on the discrimination threshold of circular, radial, and spiral GPs, partially replicating previous findings on circular GPs. Our results indicate that circular GPs are more easily perceived than radial and spiral GPs, showing lower discrimination thresholds. Furthermore, we found that discrimination thresholds vary as a function of the number of unique frames but not as a function of the pattern update rate. Specifically, coherence thresholds decreased with increasing the number of unique frames. In conclusion, our findings support the existence of spatial summation of form signals coming from the unique frames that generate complex GPs. On the other hand, they do not support temporal integration of local form-motion signals based on the pattern update rate.

Keywords: Form-motion integration, static Glass patterns, dynamic Glass patterns; complex shapes; form summation, global form.

1. Introduction

A long-standing view of visual neuroscience has considered the visual system as hierarchically organized, beginning with the primary visual cortex (V1), and separating into the ventral and dorsal streams; the first reaching area V4 and inferotemporal areas, and the second the middle temporal area (MT) and parietal areas (Gustavsen & Gallant, 2003; Mishkin et al., 1983; Ungerleider & Mishkin, 1982; Ungerleider & Haxby, 1994). These two streams have been associated with the processing of form and motion cues, respectively (Mishkin et al., 1983; Shen et al., 1999; Ungerleider & Mishkin, 1982). However, mounting experimental evidence has initiated a reevaluation of this rigid dichotomy suggesting an alternative perspective, portraying the brain as a complex and interconnected network (Amano et al., 2009; Apthorp et al., 2013; for a review see Donato et al., 2020; Edwards et al., 2013; Englund & Palomares, 2012; Fang & He, 2005; Geisler, 1999; Kourtzi et al., 2008; Krekelberg et al., 2003, 2005; Mather et al., 2012; Sheth & Young, 2016; Tang et al., 2015). In this context, Edwards et al. (2013) investigated how static orientation cues influence the spatial integration of 1D and 2D motion signals in global-Gabor and global-plaid stimuli. Local-motion information can yield either 1-dimensional (1D) or 2-dimensional (2D) solutions. Specifically, 1D signals arise when the aperture problem remains unsolved, leading to each signal representing an estimate of the local-orthogonal component of the object's motion. On the other hand, 2D signals emerge when the aperture problem is resolved, resulting in each signal representing an estimate of the object's motion. In their study, Edwards et al. (2013) found that orientation cues impact the perceived direction of global-Gabor stimuli (1D signal) but not global-plaid stimuli (2D signals). This investigation contributes to our understanding of how static orientation cues affect global motion mechanisms.

An example of the crosstalk between the dorsal and the ventral streams is given by a category of visual stimuli called dynamic Glass patterns (GPs), broadly employed to investigate how form and motion features are processed in the visual system (Barlow & Berry, 2010; Krekelberg et al., 2003; Pavan et al., 2017; Smith et al., 2002, 2007). GPs consist of pairs of dots, known as dipoles, which can be spatially arranged using geometric transformations to create various global configurations. These configurations can be categorized as either simple or complex. Simple GPs have straightforward structures, like translational patterns, representing only one dipole orientation. On the other hand, a global representation of the stimulus must be formed by integrating various dipole orientations for complex GPs, such as circular, radial, spiral, and hyperbolic patterns (Chen, 2009; Kelly et al., 2001; Nankoo et al., 2012). In this context, "simple" and "complex" are used to describe these two categories of GPs.

Moreover, GPs can be made of either a single still frame that creates *static GPs* or multiple unique frames shown in rapid succession that create *dynamic GPs* (Donato et al., 2020, 2021; Nankoo et al., 2012; Pavan et al., 2017, 2021). A peculiar characteristic of dynamic GPs is that they do not show dipole-to-dipole correspondence throughout the frames because dipoles are randomly reallocated in the space, yet they maintain a constant geometrical configuration (e.g., circular, spiral, etc.). For these characteristics, dynamic GPs evoke an illusory directional motion congruent to the dipoles' axes. Consequently, the stimulus is perceived to move translationally or circularly, although there is not an exact trajectory such as upward, downward, clockwise, or counterclockwise. In the current study, we will refer to the visual effect triggered by dynamic GPs as *non-directional motion* (Donato et al., 2021), although other studies refer to this effect as *implied motion* (Krekelberg et al., 2003, 2005; Joshi et al., 2020, 2021). We decided not to use the term implied motion because, in many studies on visual perception, this is employed to indicate implicit motion represented in static pictures, such as a photograph that displays a person or an animal in the act of running (Friedman & Stevenson, 1975; Lorteije et al., 2006; Pavan et al., 2011; Yamamoto & Miura, 2012).

Previous studies have shown that the perception of GPs varies based on their global configuration and the number of frames. Dynamic GPs have lower thresholds than static GPs, and circular GPs have lower thresholds than translational GPs (Achtman et al., 2003; Day & Palomares, 2014; Donato et al., 2021; Kurki & Saarinen, 2004; Nankoo et al., 2012, 2015). Different studies attempted to explain this perceptual difference, for example, Ohla et al. (2005) used event-related potentials (ERPs) to explore the human neurophysiological correlates of GP perception. The visual stimuli were circular, translational, and random GPs, displayed using two isoluminant hues. Participants were asked to press a button on the keypad when they saw a different color, red or violet. The authors hypothesized that the N170 component had to produce the highest ERP amplitudes for circular GPs. This hypothesis has its roots in previous studies that showed that the N170 component is associated with complex visual features, specifically, the processing of edge detection in Kanizsa figures (Herrmann & Bosch, 2001) and facial perception (Itier & Taylor, 2004). In fact, their findings revealed that circular patterns elicited a broader N170 component amplitude than translational GPs. The N170 component seems to be evoked by visual areas around V4, and previous evidence showed that V4 and the inferotemporal cortex (IT) are more sensitive to complex GPs than simple GPs (Chen, 2009; Donato et al., 2021). In fact, these cortical regions have been thought to be more sensitive to specific contour features such as acute curvature relative to the shape's center (Pasupathy & Connor, 1999, 2002; Yau et al., 2013) - probably because they are characterized by brain cells tuned to circular shapes (Desimone et al., 1984; David et al., 2006; Gallant et al., 1993, 1996; Kim et al., 2019; Pasupathy, 2006; Tanaka, 1996). However, other studies such as Hegdé & Van Essen (2007) observed different results showing that there are no significant differences in V4 in the processing of simple and complex shapes. Specifically, the authors compared shape representation in visual areas V2 and V4 and recorded monkeys' brain cell responses while they were exposed to various visual stimuli. The stimuli included 48 grating stimuli and 80 contour stimuli, grouped into subclasses based on orientation, spatial frequency, size, and shape. The aim was to investigate the selectivity of different form cues important for image segmentation and object recognition. The results revealed that V4 is not more sensitive to complex shapes than V2 (Anzai et al., 2007; Hegdé & Van Essen, 2007). In support of the evidence found by Ohla et al. (2005), there is an electrophysiological study by Pei et al. (2005), in which the authors analyzed the event-related potentials (ERPs) in response to circular, radial, translational, and random/noise GPs (i.e., the control condition). The time-averaged responses of circular and radial GPs differed more from the control condition than the responses of translational GPs.

Dynamic GPs are distinguished by their pattern update rate and the number of unique frames. These attributes play a pivotal role in generating non-directional motion (Or et al., 2007; Pavan et al., 2021; Ross et al., 2000). In a psychophysical study, Nankoo et al. (2015) focused on disentangling the role of these two factors in the perception of translational GPs. The number of unique frames and the pattern update rate were combined into a set of nine conditions, including a static condition and eight dynamic conditions. The task was a two-alternative forced choice (2AFC) where participants had to indicate whether the presented GP was coherent or not. The results suggested that the number of unique frames (but not the pattern update rate) had a key role in lowering the thresholds of GPs.

The present study examined how the number of unique frames and pattern update rate affect participants' discrimination thresholds in different types of complex GPs: concentric, radial, clockwise spiral, and counterclockwise spiral GPs. To achieve this, we used the same method as Nankoo et al. (2015). The objective was to determine whether participants' discrimination coherence thresholds for complex dynamic GPs solely depend on the number of unique frames or also on the pattern update rate. If participants' sensitivity to complex GPs depends on the number of unique frames, we should expect that coherence thresholds decrease as the number of unique frames increases; this would indicate spatial summation of multiple complex form signals across static unique frames. On the other hand, if participants' sensitivity depends on the pattern update rate, a decrease in coherence thresholds is expected as increasing the pattern update rate, regardless of the number of unique frames; this would indicate temporal integration of local motion signals as the pattern update rate increases. However, a decrease in the coherence threshold as a function of both the number of unique frames and pattern update rate would indicate the coexistence and interplay of both mechanisms in the perception of complex and dynamic patterns.

2. Methods

2.1. Participants

Sixteen individuals participated in the experiment. This sample size was determined before starting the data collection by using G*Power (Faul et al., 2007, 2009; Mayr et al., 2007) to attain a power greater than 0.9 with an effect size of 0.25. All individuals had normal vision or normal vision with correction. The experiment involved binocular viewing of the stimuli. Each participant attended four sessions on four distinct days: one session with circular GPs, one with radial GPs, one with clockwise spiral GPs, and one with counterclockwise spiral GPs. Nine females and seven males with a mean age of 22.44 years (SD: 2.65 yrs.) constituted the sample. One of the authors (MR) performed the experiment, while the remaining participants were naïve. Prior to their participation in the experiment, participants were provided with a comprehensive overview of the study to obtain their written consent. The experiment was conducted in accordance with the Declaration of Helsinki of the World Medical Association (World Medical Association, 2013). The project has been approved by the Ethics Committee for Psychological Research at the University of Padova (protocol number: 4466).

2.2. Apparatus

A 20-inch HP p1230 monitor with a spatial resolution of 1024 x 768 pixels and a refresh rate of 60 Hz was used to display the stimuli. Each pixel subtended 2.13 arcmin. All the participants sat in a dimly lit room, with their eyes 57 cm away from the screen. Matlab Psychtoolbox-3 (http://psychtoolbox.org/) was used to present the stimuli (Brainard, 1997, Kleiner et al., 2007, Pelli & Vision, 1997).

2.3.Stimuli

Circular, radial, clockwise spiral, and counterclockwise spiral GPs were utilized in the experiment as visual stimuli (see Fig. 1). All GPs were generated as ensembles of 2146 white dipoles (Michelson contrast: 0.99, density: 6%) on a black background (Donato et al., 2021; Nankoo et al., 2015). Each dot had a diameter of 0.04 deg and a distance between them of 0.25 deg. GPs were displayed in a circular window surrounded by an annulus with a maximum radius of 5.35 deg (diameter: 10.7 deg). Static GPs consisted of a single unique frame. Instead, dynamic GPs comprised two or more unique frames displayed in rapid succession (each frame had a duration of 0.0167-s). Stimuli were presented for 0.2-s. Table 1 reports the sequence and number of unique frames constituting the static and dynamic GPs that were presented, together with the relative pattern update rate (Donato et al., 2021; Nankoo et al., 2015). It should be noted that since under condition 1 the same 12 unique frames are presented for 0.2-s, the resulting update rate is 5Hz and thus the GPs are perceived as static. At the center of the circular aperture, a gray fixation point with a diameter of 0.3 degrees was constantly present.

Condition	Sequence of Unique Frames	Number of Unique Frames	Pattern Update Rate (Hz)
1	AAAAAAAAAAAA	1	5
2	ABCDEFGHIJKL	12	60
3	AAAAAABBBBBB	2	10
4	AAABBBAAABBB	2	20
5	ABABABABABAB	2	60
6	AAABBBCCCDDD	4	20
7	ABCDABCDABCD	4	60
8	AABBCCDDEEFF	6	30
9	ABCDEFABCDEF	6	60

Table 1. Temporal conditions used in the experiment. The pattern update rate (Hz) is provided together with the sequence and the number of unique frames. The arrangements of the unique frames are denoted by the letters in the second column (each letter stands for a unique frame). This grouping of unique frames and pattern update rate were the same as in Donato et al. (2021) and Nankoo et al. (2015).

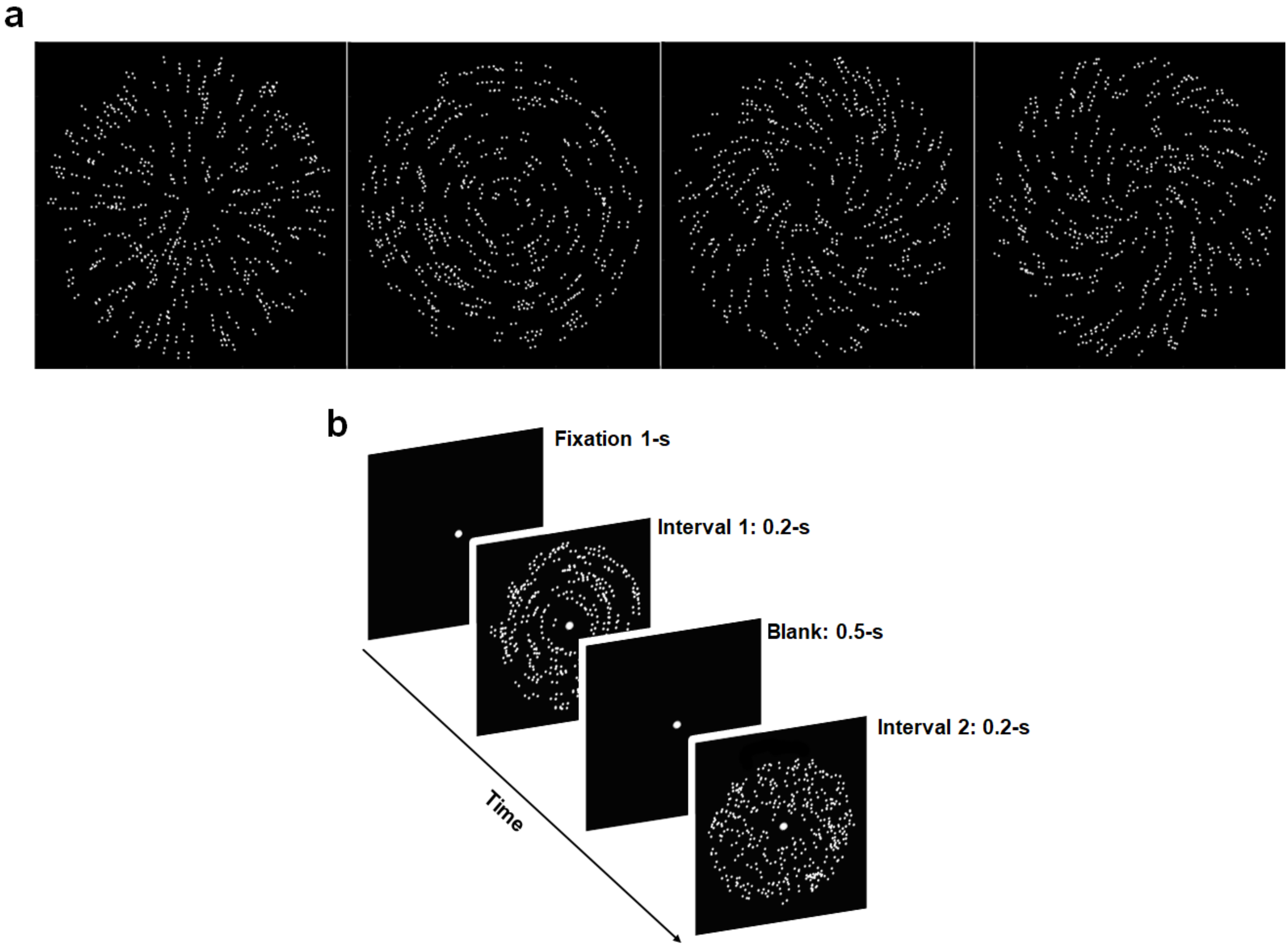

Figure 1. Representation of the stimuli (**a**) and procedure (**b**) used in the experiment. For illustration purposes, these GPs examples do not contain all the 2146 dipoles. Panel (**a**) shows the different GP types used; from left to right: radial, circular, spiral clockwise, and spiral counterclockwise. In panel (**b**) the most coherent (circular) pattern is displayed in the first temporal interval, whereas in the second interval a noise GP is displayed. The temporal interval of the coherent GP was randomized across trials. The panel only shows a circular GP, but in the experiment radial and spiral patterns were also used.

3. Procedure

Four two-hour sessions were completed by participants over four days. The four sessions adopted the same procedure but employed different types of complex dynamic GPs (i.e., either circular, radial, or spiral - clockwise and counterclockwise). The order of the four sessions was randomized across participants. At the start of each session, each participant received instructions on the type of GP displayed and completed 30 trials to become familiar with the stimulus and task. Each trial consisted of a fixation point of 1-s, two temporal intervals of 0.2-s each, and a blank interval of 0.5-s. One of the two intervals always contained a coherent GP and the other interval a noise GP (Figure 1b). The presentation order of the two intervals was randomized across trials. Observers performed a two-interval forced-choice task (2IFC) in which they had to report whether the coherent GP was displayed in the first interval by pressing the key "A" on a standard Italian computer keyboard or in the second interval by pressing the key "L". An Updated Maximum-Likelihood (UML) staircase procedure with a 1 up – 3 down rule was used for estimating participants' parameters of the psychometric function (Shen & Richards, 2012; Shen, Dai, & Richards, 2014). Each staircase terminated after 150 trials. For each participant, the coherence threshold was calculated from the best parameters of the Cumulative Gaussian estimated with the UML procedure, finding the coherence corresponding to the 79% correct performance from the psychometric function. The order of the nine temporal conditions (Table 1) was randomized among the participants and throughout the sessions.

4. Results

Figure 2 shows the discrimination thresholds as a function of number of unique frames and pattern update rate, separately for each pattern type.

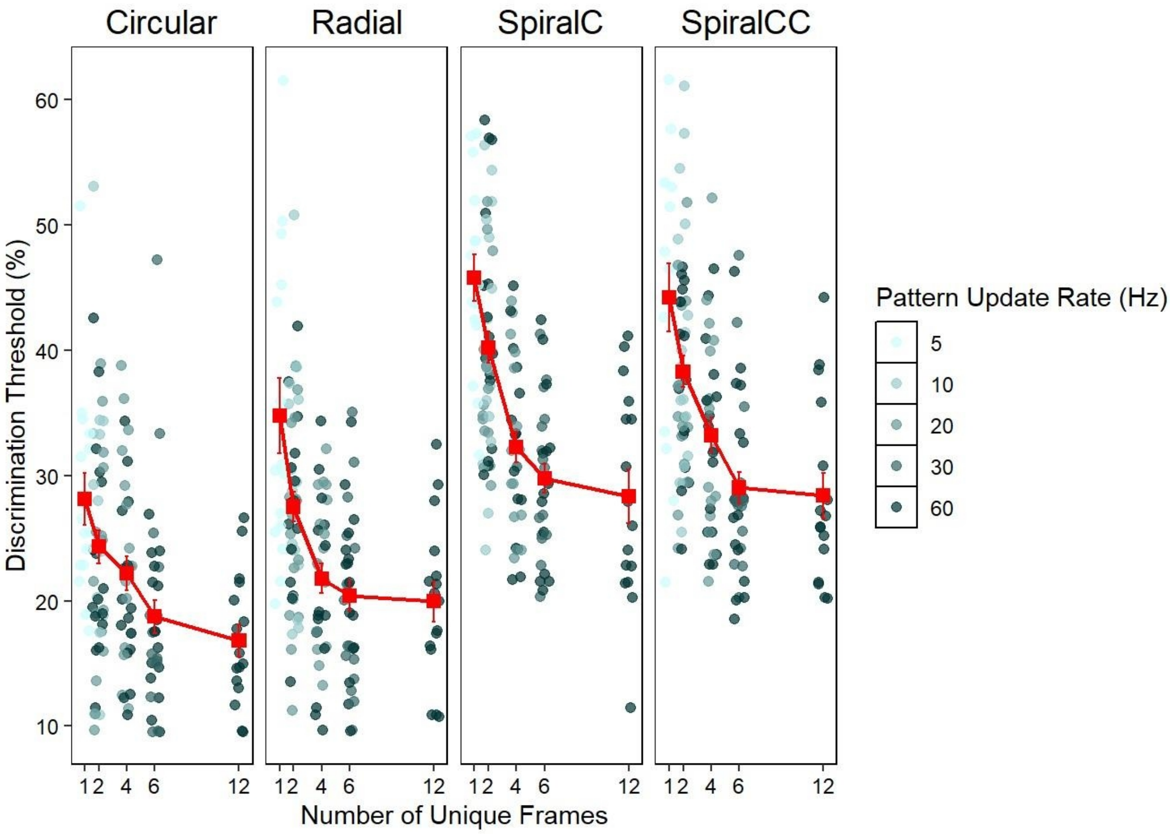

Figure 2. Individual discrimination threshold as a function of the number of unique frames for each pattern update rate. The number of unique frames is represented on the horizontal axis. The points with different colors represent the five different pattern update rates. The red squares represent the means with standard errors.

We first evaluated the shape of the distribution of the individual thresholds for each combination of pattern type and number of unique frames. No major deviations from normality were detected, as the Shapiro-Wilk test showed no statistically significant *p*-values for 16 out 20 combinations (a skewness coefficient >1 emerged for only two combinations).

The visual examination of Figure 2 indicates a potential association between the number of unique frames and/or the pattern update rate, and the discrimination threshold, which may be suitably modeled by a negative exponent power function. This conjecture was substantiated through quantitative analysis, to be expounded later in this subsection. Consequently, to have linear distributions, we implemented a logarithmic transformation on the discrimination thresholds, unique frame count, and pattern update rate.

The initial phase of the analysis examined the impact of the number of unique frames and the pattern update rate on discrimination thresholds, assessing their combined influence. As depicted in Figure 2 and corroborated by forthcoming statistical analyses, the effects of these two variables exhibited consistency across various GP types. Consequently, an initial assessment of their influence on discrimination thresholds could be conducted independently of the pattern type factor. The subsequent phase of the analysis was dedicated to investigating the influence of pattern types (i.e., circular, radial, clockwise spiral, counterclockwise spiral) on discrimination thresholds.

The lme4 package (Bates et al., 2015) was employed to fit linear mixed-effects models to the dataset. The log-likelihood ratio test was conducted using the anova() function from the lmerTest package (Kuznetsova et al., 2017). A univariate model with the number of unique frames as the fixed effect and the by-subject intercept as the random effect demonstrated a significantly superior fit to the data compared to a null model comprising solely the by-subject random intercept ($\chi^2(1) = 125.5$, $p < .001$). Incorporating the update rate as a second predictor into the model did not yield a statistically significant enhancement in model performance ($\chi^2(1) = 1.66$, $p = .197$). In contrast, augmenting the model initially featuring only the update rate with the number of unique frames as a second predictor significantly improved its performance ($\chi^2(1) = 52.55$, $p < .001$). Lastly, adding the interaction term between the number of unique frames and the update rate to the model initially featuring only the number of unique frames did not improve the model performance in a statistically significant manner ($\chi^2(2) = 1.84$, $p = .398$). These findings suggest that the discrimination threshold was influenced by the number of unique frames, while the pattern update rate showed no discernible impact.

The null model, along with the two single-predictor models, the additive model, and the interaction model, underwent comparison employing several fit indices, which were computed utilizing the *compare_performance()* function within the *easystats* package (Lüdecke et al., 2021, 2022). The relevant data can be found in Table 2. Regarding the AIC index, the results suggest a modest preference for the model with the number of unique frames as the sole predictor over the model with two predictors. A distinct advantage for the former model became evident in the comparison based on the BIC index.

Model	AIC (weights)	AICc (weights)	BIC (weights)	R^2 (conditional)	ICC	RMSE	Sigma
Null	-462.328 (< .001)	-462.286 (< .001)	-449.26 (< .001)	.194	.194	.154	.156
Update rate	-534.983 (< .001)	-534.912 (< .001)	-517.558 (< .001)	.295	.218	.144	.146
N. unique frames	-585.868 (.542)	-585.798 (.463)	-568.444 (.913)	.356	.236	.137	.139
N. unique frames + Update rate	-585.532 (.458)	-585.426 (.385)	-563.751 (.087)	.357	.236	.137	.139
N. unique frames x Update rate	-583.712 (.187)	-583.564 (.152)	-557.575	.357	.236	.137	.139

Table 2. This table presents a comparative analysis of fit indices for various statistical models, including the null model, two single-predictor models, and the additive model. Each model had a by-subject intercept as a random effect.

Following the determination that the discrimination threshold was impacted by the number of unique frames and not by the update rate, our focus shifted to examining the potential effects of the pattern type. We constructed a linear mixed-effects model for the data, incorporating the number of unique frames and the pattern type as fixed effects, with the inclusion of the by-subject intercept as a random effect. The number of frames was treated as a quantitative predictor, while the pattern type was considered a categorical predictor. This model exhibited a significantly better fit to the data when compared to the model featuring only the number of unique frames as a single predictor ($\chi^2(3) = 375.24$, $p < .001$). This finding implies a substantial influence of the pattern type on the discrimination threshold.

Introducing the interaction between these two predictors did not yield a significant enhancement in model performance ($\chi^2(3) = 1.75$, $p = .626$), indicating that the impact of the number of unique frames on the discrimination threshold remained consistent across all four pattern types. Table 3 presents the fit indices for the three models, confirming that the additive model achieved optimal performance. It is important to note that in this context we did not consider the update rate, based on the outcomes of the initial phase of the analyses.

Model	AIC (weights)	AICc (weights)	BIC (weights)	R2 (conditional)	ICC	RMSE	Sigma
N. unique frames	-585.868 (<.001)	-585.798 (<.001)	-568.444 (<.001)	.356	.236	.137	.139
N. unique frames + Pattern type	-955.106 (.893)	-954.908 (.902)	-924.613 (.999)	.669	.385	.098	.1002
N. unique frames x Pattern type	-950.861 (.107)	-950.471 (.098)	-907.3 (<.001)	.669	.384	.098	.1004

Table 3. Comparison of fit indices for three models of discrimination threshold. Model 1 includes only the number of unique frames as a predictor, Model 2 incorporates both the number of unique frames and pattern type as predictors, treating pattern type as categorical, and Model 3 is an interaction model combining both predictors. Each model had a by-subject intercept as a random effect.

Graphical assessments were conducted using the *check_model()* function within the *easystats* package (Lüdecke et al., 2021, 2022) to scrutinize the assumptions of the additive model. Noteworthy deviations from these assumptions were not observed. The data exhibited a tendency towards linear distribution, the residuals did not significantly deviate from normality ($p = .291$), no outliers were identified (Cook's distance < 0.7), and the random effects followed a normal distribution. However, a minor violation of the assumption of homoscedasticity of the residuals was detected ($p < .001$), primarily attributable to reduced variability in the thresholds for extreme values.

Utilizing the *estimate_contrast()* function within the *easystats* package (Lüdecke et al., 2021, 2022), we conducted post hoc *t*-tests, adjusted for Bonferroni correction, to compare the mean thresholds across the four pattern types. All comparisons yielded statistically significant results (ts > 4.01, ps < .001), except for the comparison between clockwise spiral and counterclockwise spiral patterns ($t(553.01) = 0.78$, $p \approx 1$). The circular pattern exhibited the lowest discrimination threshold, followed by the radial pattern, with the two spiral patterns demonstrating higher thresholds (see Figure 2). Additionally, post hoc t-tests were carried out to compare the mean thresholds among the five levels of the number of unique frames. All these comparisons reached statistical significance (ts > 4.0, ps < .004), except for the comparison between six and twelve frames ($t(553) = 1.45$, $p \approx 1$). As illustrated in Figure 2, the threshold displayed a consistent decrease with increasing the number of unique frames.

Four distinct power functions were deduced based on the parameters of the additive model:

$$Circular\ pattern: y = 29.61x^{-0.6}$$
$$Radial\ pattern: y = 30.2x^{-0.6}$$
$$Clockwise\ pattern: y = 44.67x^{-0.6}$$
$$Counterclockwise\ pattern: y = 43.65x^{-0.6}$$

where y is the discrimination threshold expressed as percentage and x is the number of unique frames. It is worth noting that the exponent remains constant throughout the four equations, which reflects the lack of interaction between the number of unique frames and the pattern type (i.e., the effect of the number of unique frames on the threshold remains consistent across the four pattern types). The effects of the pattern type are reflected in the varying parameter a in each equation.

Lastly, we conducted a comparison of three distinct models: the power function model ($y=ax^{-b}$), the exponential function model ($y = ab^x$), and the simple linear model ($y = ax+b$). Each model incorporated the pattern type and the number of unique frames as fixed effects, alongside the by-subject intercept as a random effect. In the power function model, both the threshold and the number of frames underwent log-transformation. In the exponential function model, solely the threshold underwent log-transformation, while no transformations were applied in the linear model. These non-nested models were compared solely through the fit indices presented in Table 4. The provided indices unequivocally support the power function model.

Model	AIC (weights)	BIC (weights)	R^2 (conditional)	ICC
Power	-955.1 (>.999)	-924.6 (>.999)	.669	.385
Exponential	-893.4 (<.001)	-862.9 (<.001)	.631	.358
Additive	3942.3 (<.001)	3972.8 (< .001)	.304	.304

Table 4. Comparative indices of fit for three non-nested models. This table presents a comparison of three distinct models: the power function model, the exponential function model, and the simple linear model. Each model incorporates the pattern type and the number of unique frames as fixed effects, alongside the by-subject intercept as a random effect.

Finally, it is noteworthy to mention that the same analyses performed on the thresholds were also conducted on Beta values. The results supported the null model, indicating that neither the number of unique frames nor the update rate influenced the Beta. The type of pattern appeared to have an influence, albeit weak, on the Beta values. Specifically, upon examining the confidence intervals, it was observed that circular GPs had the highest Beta values, suggesting that participants were more sensitive or better at discriminating circular GPs. In contrast, counterclockwise spiral GPs, and especially clockwise spiral GPs, exhibited the lowest Beta values. Radial GPs had Beta values lower than circular GPs and higher than counterclockwise and clockwise spiral GPs. Subsequent post hoc comparisons showed that the only statistically significant difference was between circular GPs and clockwise spiral GPs. Due to the strong negative skewness in the Beta values distributions, an additional analysis was performed on the inverse-log transformed Beta values. The results were substantially equivalent to those of the analysis performed on untransformed values, confirming the overall reliability and robustness of the main findings.

5. Discussion

In the last decades, dynamic GPs have been largely used to provide evidence in support of the interaction between the ventral and the dorsal streams in the visual system (for a review, see Donato et al., 2020). Simple and complex global configurations in GPs can be easily detected when dipoles are coherently displayed. Global perception in static and dynamic GPs depends dramatically on integration mechanisms that combine local features (i.e., dipoles orientation) into a global percept (Day & Palomares, 2014; Prazdny, 1986). Previous studies showed that the perception of dynamic GPs is significantly affected by specific spatial and temporal characteristics such as inter-dipoles distance (or dipoles density), luminance contrast, pattern update rate, etc. (Day & Palomares, 2014; Donato et al., 2021; Lin et al., 2017; Nankoo et al., 2015; Palomares et al., 2010; Pradzny, 1984; Wilson et al., 2004). Even though some studies explored how spatial and temporal cues influence dynamic GPs perception, the mechanisms of temporal and spatial summation across multiple frames in complex dynamic GPs have not been fully examined. In the current study, we addressed this question by investigating the role of the pattern update rate and the number of unique frames in the perception of complex GPs, respectively circular, radial, spiral clockwise, and spiral counterclockwise. We found that circular GPs have lower discrimination thresholds compared to the other complex configurations tested, specifically radial, spiral clockwise, and counterclockwise. Conversely, spiral GPs, either clockwise or counterclockwise, were the most difficult to perceive, showing the highest discrimination thresholds, a result in line with previous studies (Nankoo et al., 2012; Seu and Ferrera, 2001; Schmidtmann et al., 2015). For example, Seu and Ferrera (2001) tested participants' detection thresholds over three types of complex GPs – i.e., circular, radial, and spiral. Participants were asked to indicate which of the two intervals presented on the screen contained the coherent GP (signal range 0-50%) while the other interval contained a random/noise GP (signal range 0%). The authors found that spiral GPs have the highest detection thresholds compared to circular and radial GPs, meaning that this was the most difficult configuration to detect. This result can be explained through the hypothesis of symmetry (Mach, 1914) according to which radial and circular GPs are characterized by infinite symmetry axes, yet the same does not apply to spiral GPs. Lines of symmetry can be positively correlated with better sensitivity for radial and circular configurations (Seu and Ferrera, 2001). Another study by Kelly et al. (2001) compared the detection threshold of circular, radial, and translational GPs in human participants and pigeons. In both humans and pigeons, the detection thresholds degraded when noise (i.e., random dipoles) increased. However, pigeons showed the same detection thresholds trend among the three configurations, whereas humans showed the highest thresholds (i.e., the worst performance) in detecting translational GPs - this pointed to a different form processing between humans and pigeons.

Interestingly, a similar pattern of results is shown by another class of visual stimuli called random dot kinematograms (RDKs) (Morrone et al., 1999). RDKs are made of single dots that, differently from GPs, follow a precise trajectory throughout the frames. Morrone et al. (1999) measured the detection thresholds for spiral RDKs and circular RDKs that induced a percept of expansion or contraction. They found that spiral RDKs were the most difficult pattern to detect. This evidence leads to thinking that RDKs and GPs might share an overlapping neural network that processes similarly complex configurations.

Moreover, our results confirmed previous evidence indicating that static GPs are more difficult to discriminate than dynamic GPs regardless of the temporal condition, even in the case of complex configurations (Burr & Ross, 2006; Donato et al., 2020, 2021; Joshi et al., 2020; Joshi et al., 2021; Nankoo et al., 2012, 2015; Pavan et al., 2017, 2021; Van Grootel et al., 2017). Our investigation aligns with the observations made by Nankoo et al. (2015) regarding translational GPs. Their study reveals a consistent pattern, where the condition involving two unique frames emerges as the most problematic. Parallel to their observations, our data also indicates that increasing the update rate beyond 20 Hz does not yield benefits, with the 60 Hz rate exhibiting poorer performance compared to lower rates. This trend is specific to the configuration with two unique frames, as opposed to configurations with four, six, and twelve unique frames, which still demonstrate advantages with higher update rates. Remarkably, the GPs with a 60 Hz update rate were the least effective for the condition with two unique frames, extending beyond the translational GPs explored by Nankoo et al. (2015) and encompassing all four GP types examined in our study. Additionally, we previously conducted a study (Pavan et al., 2021) to psychophysically investigate the level at which global orientation is extracted from translational GPs using the tilt after-effect (TAE) and manipulating the spatiotemporal properties of the adapting pattern. The TAE is a visual phenomenon where prolonged exposure to a pattern or stimulus tilted in a particular direction leads to a perceptual distortion in the opposite direction when subsequently viewing a neutral pattern. Essentially, it causes an optical illusion of tilt in the opposite direction from the original stimulus. In that study, we found that the TAE peaked at a temporal frequency of ~30 Hz, suggesting that orientation-selective units responding to translational GPs are sensitive to high temporal frequencies. Moreover, the TAE from translational GPs peaked at lower spatial frequencies than the dipoles' spatial constant. These effects are consistent with form-motion integration at low and intermediate levels of visual processing.

We also found a significant influence of the number of unique frames (i.e., spatial information) on the perception of complex GPs suggesting that spatial summation of form signals shapes the perception of dynamic complex GPs regardless of the patterns' configuration and the frequency of presentation of the frame sequence. Spatial summation is the ability of the visual system to integrate different visuospatial information that, in our case, comes from the number of different dipoles presented across the sequence of unique frames composing the GP. Previous studies explored spatial summation manipulating the size of the signal area instead of the number of frames forming the stimulus and demonstrated that circular GPs show a stronger spatial summation compared to translational GPs (Wilson et al 1997; Wilson & Wilkinson, 1998). Wilson and Wilkinson (1998) aimed to study global form processing and spatial summation in translational, circular, radial, and hyperbolic GPs. GPs were split into eight pie-shaped segments alternating either random dipoles or coherently oriented dipoles with a small number of random dipoles. Separately, they also used a GP divided into an outer annulus with noise dipoles and an inner annulus with signal dipoles to estimate the pooling mechanisms by varying the radius at which the shift between noise and coherent dipoles occurred. Participants were asked to perform a two-interval forced-choice task in which they had to indicate whether the coherent GP was contained in the first or in the second interval – the remaining interval contained the noise GP with random dipoles orientation. In this study, Wilson & Wilkinson (1998) hypothesized that form processing is the result of an articulated process of coding, filtering, and linear summation that involves the various visual areas hierarchically. According to this model, there are three main levels according to which orientation signal is processed: a first level of coding and filtering of individual orientation signals, a second level of noise filtration and correction of the processed signal, and finally a third level of integration and spatial summation of the signals coded and selected in the previous steps. These three levels of processing take place respectively in V1, V2, and finally V4 - a system of increasing specialization as proposed by Ostwald and colleagues (2008).

However, Schmidtmann et al. (2015) pointed out that spatial summation in circular GPs is not additive (of which linear summation is a special case) but probabilistic. Their general aim was to investigate the summation mechanisms for different oriented textures including circular, radial, spiral, and translational GPs. They tested whether oriented textures are processed according to probability summation (PS) or additive summation (AS) (Kurki et al., 2003; Wilson et al., 1997; Wilson & Wilkinson, 1998). The main assumption of AS is that various stimulus features add together in a unified mechanism (Kingdom et al., 2015; Kingdom & Prins, 2016). In the case of linear summation, it predicts that the features of a stimulus are linearly combined (Kingdom & Prins, 2016). On the other hand, PS assumes that the different channels or mechanisms responsible for detecting stimuli operate independently of each other. In other words, the response of one channel does not affect the response of another. According to this model, the increased probability of detecting a stimulus in the presence of multiple stimuli is due to the greater likelihood that at least one of the stimuli will either exceed the threshold or produce the strongest signal, thus enhancing the overall detection performance (Kingdom et al., 2015; Kingdom & Prins, 2016). PS, however, has not been fully tested to explain spatial summation. AS and PS have been treated in the context of two broad theories, the Signal Detection Theory (SDT) and High-Threshold Theory (HTT). HTT was described by Quick (1974) to analyze how we detect specific signals. It assumes the existence of a fixed and notably high detection threshold, rendering stimuli below this threshold invisible (Kingdom & Prins, 2016). Differently, according to the SDT there is not a fixed threshold value that influences the detection process; however, it proposes that perceptual decisions rely on an internal representation that follows a sampling distribution with specific mean and variance. These two features play a crucial role in determining how easily we can differentiate one stimulus from others (Kingdom & Prins, 2016). Schmidtmann et al. (2015) measured the signal-to-noise ratio needed for detection while varying the size of the signal area, with the remaining area containing noise (i.e., random dipoles/Gabors orientations). The task was to determine which of the two successively presented stimulus arrays contained the target texture using the method of constant stimuli. One of the stimuli consisted of noise only, whereas the other contained a variable fraction of coherent orientation. The authors found that the degree of summation was not additive or linear and GPs detection sensitivity was not linked to the configuration used. Therefore, their study did not support the hypothesis of specialized detectors for circular configurations and showed that probability summation explains the mechanisms underlying circular, radial, spiral, and translational GPs detection. This topic continues to be a matter of debate due to a recent investigation conducted by Green and colleagues in 2018, which examined radial frequency patterns and indicated that the most accurate description for global shape processing is the AS. Therefore, the mechanisms of integration of local form cues into a global coherent percept remains a topic of ongoing investigation with no definitive consensus regarding the existence of dedicated global form detectors. However, it is important to note that the primary focus of the present study differs from investigating summation types (i.e., additive, or probabilistic).

In conclusion, our study sheds light on several aspects of complex GPs processing - first and foremost, our findings support the notion that circular configurations in GPs are inherently easier to perceive than spiral and radial, and that dynamic GPs are easier to discriminate than static GPs. Interestingly, our study suggests that the pattern update rate may not play a pivotal role in the perception of complex GPs. Finally, our findings not only contribute to our understanding of complex GP perception but also underscore the necessity for continued investigation in this field. Exploring new insights into spatial and temporal processing in GPs and testing additional combinations and interactions between pattern update rates and unique frames is essential to provide a more nuanced understanding of their potential effects.

6. Conclusions

In conclusion, our findings demonstrate that form information given by dipoles' orientation in complex GPs is summed throughout the frames and this helps the human visual system to discriminate coherent and complex GPs from noise GPs. However, the rate at which this process occurs does not seem to play a crucial role in discriminating complex global configurations in GPs. Lastly, our study confirms that dynamic GPs are easier to detect than static GPs and circular GPs are the easiest to detect compared to spiral and radial GPs.

Acknowledgments

This work was carried out within the scope of the project "Use-inspired basic research", for which the Department of General Psychology of the University of Padova has been recognized as "Dipartimento di Eccellenza" by the Ministry of University and Research. MR and RD were supported by the University of Padova, Department of Psychology, and by the Human Inspired Centre.

Conflict of interest

The authors declare no competing financial interests.

Data availability

The data presented in this study are openly available in Open Science Framework (OSF) at https://osf.io/5x3gy/?view_only=c108b1c0caf945d0bd68d08eab7b1f40.

Authors contributions

MR: Conceptualization, Methodology, Data curation, Writing - original draft, Writing - review & editing. **GC:** Supervision, Conceptualization, Methodology, Writing - original draft, Writing - review & editing. **MV:** Data curation, Writing - original draft, Writing - review & editing. **RD:** Methodology, Writing - original draft, Writing - review & editing. **AP:** Conceptualization, Methodology, Software, Data curation, Writing - original draft, Supervision, Writing - review & editing.

References

Achtman, R. L., Hess, R. F., & Wang, Y. Z. (2003). Sensitivity for global shape detection. *Journal of Vision*, *3*(10), 4. https://doi.org/10.1167/3.10.4

Alais, D., Apthorp, D., Karmann, A., & Cass, J. (2011). Temporal Integration of Movement: The Time-Course of Motion Streaks Revealed by Masking. *PLoS ONE*, *6*(12), e28675. https://doi.org/10.1371/journal.pone.0028675

Amano, K., Edwards, M., Badcock, D. R., & Nishida, S. (2009). Adaptive pooling of visual motion signals by the human visual system revealed with a novel multi-element stimulus. Journal of vision, 9(3), 1–25. https://doi.org/10.1167/9.3.4

Apthorp, D., Schwarzkopf, D. S., Kaul, C., Bahrami, B., Alais, D., & Rees, G. (2013). Direct evidence for encoding of motion streaks in human visual cortex. *Proceedings of the Royal Society B: Biological Sciences*, *280*(1752), 20122339. https://doi.org/10.1098/rspb.2012.2339

Bair, W. (2004). Adaptive Temporal Integration of Motion in Direction-Selective Neurons in Macaque Visual Cortex. *Journal of Neuroscience*, *24*(33), 7305–7323. https://doi.org/10.1523/jneurosci.0554-04.2004

Barlow, H., & Berry, D. L. (2010). Cross- and auto-correlation in early vision. *Proceedings of the Royal Society B: Biological Sciences*, *278*(1714), 2069–2075. https://doi.org/10.1098/rspb.2010.2170

Bates, D., Machler, M., Bolker, B. M., & Walker, S. C. (2015). Fitting Linear Mixed-Effects Models Using lme4. *Journal of Statistical Software*, *67*(1), 1-48. https://doi.org/10.18637/jss.v067.i01

Bell, J., & Badcock, D. R. (2008). Luminance and contrast cues are integrated in global shape detection with contours. *Vision research*, *48*(21), 2336–2344. https://doi.org/10.1016/j.visres.2008.07.015

Brainard, D. H. (1997). The Psychophysics Toolbox. *Spatial Vision*, *10*(4), 433–436. https://doi.org/10.1163/156856897x00357

Burr, D., & Ross, J. (2006). The effects of opposite-polarity dipoles on the detection of Glass patterns. *Vision Research*, *46*(6–7), 1139–1144. https://doi.org/10.1016/j.visres.2005.09.018

Chen C. C. (2009). A masking analysis of glass pattern perception. *Journal of vision*, *9*(12), 1–11. https://doi.org/10.1167/9.12.22

Cook, R. Dennis. "Detection of influential observation in linear regression." Technometrics 19, no. 1 (1977): 15-18. https://doi.org/10.1080/00401706.1977.10489493

David, S. V., Hayden, B. Y., & Gallant, J. L. (2006). Spectral receptive field properties explain shape selectivity in area V4. *Journal of neurophysiology*, *96*(6), 3492–3505. https://doi.org/10.1152/jn.00575.2006

Day, A. M., & Palomares, M. (2014). How temporal frequency affects global form coherence in Glass patterns. *Vision Research*, *95*, 18–22. https://doi.org/10.1016/j.visres.2013.11.009

Desimone, R., Albright, T. D., Gross, C. G., & Bruce, C. (1984). Stimulus-selective properties of inferior temporal neurons in the macaque. *The Journal of neuroscience : the official journal of the Society for Neuroscience*, *4*(8), 2051–2062. https://doi.org/10.1523/JNEUROSCI.04-08-02051.1984

Dickinson, J. E., Han, L., Bell, J., & Badcock, D. R. (2010). Local motion effects on form in radial frequency patterns. *Journal of vision*, *10*(3), 1–15. https://doi.org/10.1167/10.3.20

Dickinson, J. E., McGinty, J., Webster, K. E., & Badcock, D. R. (2012). Further evidence that local cues to shape in RF patterns are integrated globally. *Journal of vision*, *12*(12), 16. https://doi.org/10.1167/12.12.16

Donato, R., Pavan, A., Almeida, J., Nucci, M., & Campana, G. (2021). Temporal characteristics of global form perception in translational and circular Glass patterns. *Vision Research*, *187*, 102–109. https://doi.org/10.1016/j.visres.2021.06.003

Donato, R., Pavan, A., & Campana, G. (2020). Investigating the Interaction Between Form and Motion Processing: A Review of Basic Research and Clinical Evidence. *Frontiers in Psychology*, *11*. https://doi.org/10.3389/fpsyg.2020.566848

Edwards, M., & Crane, M. F. (2007). Motion streaks improve motion detection. Vision research, 47(6), 828–833. https://doi.org/10.1016/j.visres.2006.12.005

Edwards, M., Cassanello, C. R., Badcock, D. R., & Nishida, S. (2013). Effect of form cues on 1D and 2D motion pooling. *Vision research*, *76*, 94–104. https://doi.org/10.1016/j.visres.2012.10.015

Englund, J. A., & Palomares, M. (2012). The relationship of global form and motion detection to reading fluency. *Vision Research*, *67*, 14–21. https://doi.org/10.1016/j.visres.2012.06.020

Fang, F., & He, S. (2005). Cortical responses to invisible objects in the human dorsal and ventral pathways. *Nature Neuroscience*, *8*(10), 1380–1385. https://doi.org/10.1038/nn1537

Faul, F., Erdfelder, E., Buchner, A., & Lang, A. G. (2009). Statistical power analyses using G*Power 3.1: Tests for correlation and regression analyses. *Behavior Research Methods*, *41*(4), 1149–1160. https://doi.org/10.3758/brm.41.4.1149

Faul, F., Erdfelder, E., Lang, A. G., & Buchner, A. (2007). G*Power 3: A flexible statistical power analysis program for the social, behavioral, and biomedical sciences. *Behavior Research Methods*, *39*(2), 175–191. https://doi.org/10.3758/bf03193146

Feczko, E., Shulman, G. L., Petersen, S. E., & Pruett, J. R., Jr (2014). Interactions between concentric form-from-structure and face perception revealed by visual masking but not adaptation. *Journal of vision*, *14*(2), 15. https://doi.org/10.1167/14.2.15

Friedman, S. L., & Stevenson, M. B. (1975). Developmental changes in the understanding of implied motion in two-dimensional pictures. *Child development*, *46*(3), 773–778. https://doi.org/10.2307/1128578

Gallant, J. L., Braun, J., & Van Essen, D. C. (1993). Selectivity for polar, hyperbolic, and Cartesian gratings in macaque visual cortex. *Science (New York, N.Y.)*, *259*(5091), 100–103. https://doi.org/10.1126/science.8418487

Gallant, J. L., Connor, C. E., Rakshit, S., Lewis, J. W., & Van Essen, D. C. (1996). Neural responses to polar, hyperbolic, and Cartesian gratings in area V4 of the macaque monkey. *Journal of neurophysiology*, *76*(4), 2718–2739. https://doi.org/10.1152/jn.1996.76.4.2718

Geisler, W. S. (1999). Motion streaks provide a spatial code for motion direction. *Nature*, *400*(6739), 65–69. https://doi.org/10.1038/21886

Green, R. J., Dickinson, J. E., & Badcock, D. R. (2018). Convergent evidence for global processing of shape. *Journal of vision*, *18*(7), 7. https://doi.org/10.1167/18.7.7

Gustavsen, K., & Gallant, J. L. (2003). Shape Perception: Complex Contour Representation in Visual Area V4. *Current Biology*, *13*(6), R234–R235. https://doi.org/10.1016/s0960-9822(03)00159-3

Hegdé, J., & Van Essen, D. C. (2007). A comparative study of shape representation in macaque visual areas v2 and v4. *Cerebral cortex (New York, N.Y. : 1991)*, *17*(5), 1100–1116. https://doi.org/10.1093/cercor/bhl020

Herrmann, C. S., & Bosch, V. (2001). Gestalt perception modulates early visual processing. *Neuroreport*, *12*(5), 901–904. https://doi.org/10.1097/00001756-200104170-00007

Itier, R. J., & Taylor, M. J. (2004). N170 or N1? Spatiotemporal differences between object and face processing using ERPs. *Cerebral cortex (New York, N.Y. : 1991)*, *14*(2), 132–142. https://doi.org/10.1093/cercor/bhg111

Joshi, M. R., Simmers, A. J., & Jeon, S. T. (2020). Implied Motion From Form Shows Motion Aids the Perception of Global Form in Amblyopia. *Investigative Opthalmology &Amp; Visual Science*, *61*(5), 58. https://doi.org/10.1167/iovs.61.5.58

Joshi, M. R., Simmers, A. J., & Jeon, S. T. (2021). The interaction of global motion and global form processing on the perception of implied motion: An equivalent noise approach. *Vision Research*, *186*, 34–40. https://doi.org/10.1016/j.visres.2021.04.006

Kelly, D. M., Bischof, W. F., Wong-Wylie, D. R., & Spetch, M. L. (2001). Detection of Glass Patterns by Pigeons and Humans: Implications for Differences in Higher-Level Processing. *Psychological Science*, *12*(4), 338–342. https://doi.org/10.1111/1467-9280.00362

Kim, T., Bair, W., & Pasupathy, A. (2019). Neural Coding for Shape and Texture in Macaque Area V4. *The Journal of neuroscience : the official journal of the Society for Neuroscience*, *39*(24), 4760–4774. https://doi.org/10.1523/JNEUROSCI.3073-18.2019

Kingdom, F. A., Baldwin, A. S., & Schmidtmann, G. (2015). Modeling probability and additive summation for detection across multiple mechanisms under the assumptions of signal detection theory. *Journal of vision*, *15*(5), 1. https://doi.org/10.1167/15.5.1

Kingdom, F. A. A., & Prins, N. (2016). *Psychophysics: A Practical Introduction*, 2nd Edn. Cambridge, MA: Academic Press.

Kleiner, M., Brainard, D.H., Pelli, D.G., Broussard, C., Wolf, T., Niehorster, D., (2007). What's new in Psychtoolbox-3? *Perception*. https://doi.org/10.1068/v070821.

Kourtzi, Z., Krekelberg, B., & van Wezel, R. J. (2008). Linking form and motion in the primate brain. *Trends in Cognitive Sciences*, *12*(6), 230–236. https://doi.org/10.1016/j.tics.2008.02.013

Krekelberg, B., Dannenberg, S., Hoffmann, K. P., Bremmer, F., & Ross, J. (2003). Neural correlates of implied motion. *Nature*, *424*(6949), 674–677. https://doi.org/10.1038/nature01852

Krekelberg, B., Vatakis, A., & Kourtzi, Z. (2005). Implied Motion From Form in the Human Visual Cortex. *Journal of Neurophysiology*, *94*(6), 4373–4386. https://doi.org/10.1152/jn.00690.2005

Kurki, I., & Saarinen, J. (2004). Shape perception in human vision: specialized detectors for concentric spatial structures? *Neuroscience Letters*, *360*(1–2), 100–102. https://doi.org/10.1016/j.neulet.2004.01.053

Kurki, I., Laurinen, P., Peromaa, T., & Saarinen, J. (2003). Spatial integration in Glass patterns. *Perception*, *32*(10), 1211–1220. https://doi.org/10.1068/p5102

Kuznetsova, A., Brockhoff, P. B., & Christensen, R. H. (2017). lmerTest package: tests in linear mixed effects models. *Journal of statistical software*, *82*, 1-26. https://doi.org/10.18637/jss.v082.i13

Lin, Y. S., Cho, P. C., & Chen, C. C. (2017). Contrast gain control determines global form percept in tripole Glass patterns. *Journal of Vision*, *17*(5), 2. https://doi.org/10.1167/17.5.2

Lorteije, J. A., Kenemans, J. L., Jellema, T., van der Lubbe, R. H., de Heer, F., & van Wezel, R. J. (2006). Delayed response to animate implied motion in human motion processing areas. *Journal of cognitive neuroscience*, *18*(2), 158–168. https://doi.org/10.1162/089892906775783732

Lüdecke, Daniel, Mattan S. Ben-Shachar, Indrajeet Patil, Philip Waggoner, and Dominique Makowski. "performance: An R package for assessment, comparison and testing of statistical models." *Journal of Open Source Software* 6, no. 60 (2021).

Lüdecke, D., Ben-Shachar, M. S., Patil, I., Wiernik, B. M., & Makowski, D. (2022). easystats: Framework for easy statistical modeling, visualization, and reporting. Repository CRAN. https://easystats.github.io/easystats/

Mach, E. (1914). *The analysis of sensations, and the relation of the physical to the psychical*. Open Court Publishing Company.

Mather, G., Pavan, A., Bellacosa Marotti, R., Campana, G., & Casco, C. (2013). Interactions between motion and form processing in the human visual system. Frontiers in computational neuroscience, 7, 65. https://doi.org/10.3389/fncom.2013.00065

Mather, G., Pavan, A., Bellacosa, R. M., & Casco, C. (2012). Psychophysical evidence for interactions between visual motion and form processing at the level of motion integrating receptive fields. *Neuropsychologia*, *50*(1), 153–159. https://doi.org/10.1016/j.neuropsychologia.2011.11.013

Mayr, S., Erdfelder, E., Buchner, A., & Faul, F. (2007). A short tutorial of GPower. *Tutorials in Quantitative Methods for Psychology*, *3*(2), 51–59. https://doi.org/10.20982/tqmp.03.2.p051

Mishkin, M., Ungerleider, L. G., & Macko, K. A. (1983). Object vision and spatial vision: two cortical pathways. *Trends in Neurosciences*, *6*, 414–417. https://doi.org/10.1016/0166-2236(83)90190-x

Morrone, M. C., Burr, D. C., Di Pietro, S., & Stefanelli, M. A. (1999). Cardinal directions for visual optic flow. *Current Biology*, *9*(14), 763–766. https://doi.org/10.1016/s0960-9822(99)80338-8

Nankoo, J. F., Madan, C. R., Spetch, M. L., & Wylie, D. R. (2012). Perception of dynamic Glass patterns. *Vision Research*, *72*, 55–62. https://doi.org/10.1016/j.visres.2012.09.008

Nankoo, J. F., Madan, C. R., Spetch, M. L., & Wylie, D. R. (2015). Temporal summation of global form signals in dynamic Glass patterns. *Vision Research*, *107*, 30–35. https://doi.org/10.1016/j.visres.2014.10.033

Ohla, K., Busch, N. A., Dahlem, M. A., & Herrmann, C. S. (2005). Circles are different: The perception of Glass patterns modulates early event-related potentials. *Vision Research*, *45*(20), 2668–2676. https://doi.org/10.1016/j.visres.2005.03.015

Or, C. C., Khuu, S. K., & Hayes, A. (2007). The role of luminance contrast in the detection of global structure in static and dynamic, same- and opposite-polarity, Glass patterns. Vision research, 47(2), 253–259. https://doi.org/10.1016/j.visres.2006.10.010

Palomares, M., Pettet, M., Vildavski, V., Hou, C., & Norcia, A. (2010). Connecting the Dots: How Local Structure Affects Global Integration in Infants. *Journal of Cognitive Neuroscience*, *22*(7), 1557–1569. https://doi.org/10.1162/jocn.2009.21323

Pasupathy A. (2006). Neural basis of shape representation in the primate brain. *Progress in brain research*, *154*, 293–313. https://doi.org/10.1016/S0079-6123(06)54016-6

Pasupathy, A., & Connor, C. E. (1999). Responses to contour features in macaque area V4. *Journal of neurophysiology*, *82*(5), 2490–2502. https://doi.org/10.1152/jn.1999.82.5.2490

Pasupathy, A., & Connor, C. E. (2001). Shape representation in area V4: position-specific tuning for boundary conformation. *Journal of neurophysiology*, *86*(5), 2505–2519. https://doi.org/10.1152/jn.2001.86.5.2505

Pavan, A., Ghin, F., Donato, R., Campana, G., & Mather, G. (2017). The neural basis of form and form-motion integration from static and dynamic translational Glass patterns: A rTMS investigation. *NeuroImage*, *157*, 555–560. https://doi.org/10.1016/j.neuroimage.2017.06.036

Pavan, A., Contillo, A., Ghin, F., Donato, R., Foxwell, M. J., Atkins, D. W., Mather, G., & Campana, G. (2021). Spatial and temporal selectivity of translational Glass patterns assessed with the tilt after-effect. *I-Perception*, *12*(3), 204166952110179. https://doi.org/10.1177/20416695211017924

Pavan, A., Cuturi, L. F., Maniglia, M., Casco, C., & Campana, G. (2011). Implied motion from static photographs influences the perceived position of stationary objects. *Vision research*, *51*(1), 187–194. https://doi.org/10.1016/j.visres.2010.11.004

Pei, F., Pettet, M. W., Vildavski, V. Y., & Norcia, A. M. (2005). Event-related potentials show configural specificity of global form processing. *NeuroReport*, *16*(13), 1427–1430. https://doi.org/10.1097/01.wnr.0000177003.12322.9b

Pelli, D. G. (1997). The VideoToolbox software for visual psychophysics: transforming numbers into movies. *Spatial Vision*, *10*(4), 437–442. https://doi.org/10.1163/156856897x00366

Prazdny, K. (1984). On the Perception of Glass Patterns. *Perception*, *13*(4), 469–478. https://doi.org/10.1068/p130469

Prazdny, K. (1986). Some new phenomena in the perception of glass patterns. *Biological Cybernetics*, *53*(3), 153–158. https://doi.org/10.1007/bf00342883

Quick R. F., Jr (1974). A vector-magnitude model of contrast detection. *Kybernetik*, *16*(2), 65–67. https://doi.org/10.1007/BF00271628

RCore Team. R: A Language and Environment for Statistical Computing; R Foundation for Statistical Computing: Vienna, Austria, 2021. Available online: http://www.R-project.org (March 2022).

Ross, J., Badcock, D. R., & Hayes, A. (2000). Coherent global motion in the absence of coherent velocity signals. Current biology : CB, 10(11), 679–682. https://doi.org/10.1016/s0960-9822(00)00524-8

RStudio Team. RStudio: Integrated Development for R; RStudio, Inc.: Boston, MA, USA, 2021.

Schmidtmann, G., Kennedy, G. J., Orbach, H. S., & Loffler, G. (2012). Non-linear global pooling in the discrimination of circular and non-circular shapes. *Vision research*, *62*, 44–56. https://doi.org/10.1016/j.visres.2012.03.001

Schmidtmann, G., Jennings, B. J., Bell, J., & Kingdom, F. A. A. (2015). Probability, not linear summation, mediates the detection of concentric orientation-defined textures. *Journal of Vision*, *15*(16), 6. https://doi.org/10.1167/15.16.6

Seu, L., & Ferrera, V. P. (2001). Detection thresholds for spiral Glass patterns. *Vision Research*, *41*(28), 3785–3790. https://doi.org/10.1016/s0042-6989(01)00235-8

Shen, Y., Dai, W., & Richards, V. M. (2014). A MATLAB toolbox for the efficient estimation of the psychometric function using the updated maximum-likelihood adaptive procedure. *Behavior Research Methods*, *47*(1), 13–26. https://doi.org/10.3758/s13428-014-0450-6

Shen, Y., & Richards, V. M. (2012). A maximum-likelihood procedure for estimating psychometric functions: Thresholds, slopes, and lapses of attention. *The Journal of the Acoustical Society of America*, *132*(2), 957–967. https://doi.org/10.1121/1.4733540

Shen, L., Hu, X., Yacoub, E., & Ugurbil, K. (1999). Neural correlates of visual form and visual spatial processing. *Human brain mapping*, *8*(1), 60–71. https://doi.org/10.1002/(SICI)1097-0193(1999)8:1<60::AID-HBM5>3.0.CO;2-6

Sheth, B. R., & Young, R. (2016). Two visual pathways in primates based on sampling of space: exploitation and exploration of visual information. *Frontiers in Integrative Neuroscience*, *10*. https://doi.org/10.3389/fnint.2016.00037

Smith, M. A., Bair, W., & Movshon, J. A. (2002). Signals in Macaque Striate Cortical Neurons that Support the Perception of Glass Patterns. *The Journal of Neuroscience*, *22*(18), 8334–8345. https://doi.org/10.1523/jneurosci.22-18-08334.2002

Smith, M. A., Kohn, A., & Movshon, J. A. (2007). Glass pattern responses in macaque V2 neurons. *Journal of Vision*, *7*(3), 5. https://doi.org/10.1167/7.3.5

Tanaka K. (1996). Inferotemporal cortex and object vision. *Annual review of neuroscience*, *19*, 109–139. https://doi.org/10.1146/annurev.ne.19.030196.000545

Tang, M. F., Dickinson, J. E., Visser, T. A., Edwards, M., & Badcock, D. R. (2015). Role of form information in motion pooling and segmentation. Journal of vision, 15(15), 19. https://doi.org/10.1167/15.15.19

Ungerleider, L. G., & Mishkin, M. (1982). Two cortical visual systems. In *Analysis of Visual Behavior*.

Ungerleider, L. G., & Haxby, J. V. (1994). 'What'and 'where'in the human brain. *Current opinion in neurobiology*, *4*(2), 157-165. https://doi.org/10.1016/0959-4388(94)90066-3

Van Grootel, T. J., Meeson, A., Munk, M. H. J., Kourtzi, Z., Movshon, J. A., Logothetis, N. K., & Kiorpes, L. (2017). Development of visual cortical function in infant macaques: A BOLD fMRI study. *PLOS ONE*, *12*(11), e0187942. https://doi.org/10.1371/journal.pone.0187942

Wilson, H. R., & Wilkinson, F. (1998). Detection of global structure in Glass patterns: implications for form vision. *Vision Research*, *38*(19), 2933–2947. https://doi.org/10.1016/s0042-6989(98)00109-6

Wilson, H. R., Wilkinson, F., & Asaad, W. (1997). Concentric orientation summation in human form vision. *Vision Research*, *37*(17), 2325–2330. https://doi.org/10.1016/s0042-6989(97)00104-1

Wilson, J. A., Switkes, E., & De Valois, R. L. (2004). Glass pattern studies of local and global processing of contrast variations. *Vision research*, *44*(22), 2629–2641. https://doi.org/10.1016/j.visres.2003.06.001

World Medical Association, 2013. World Medical Association Declaration of Helsinki. Ethical Principles for Medical Research Involving Human Subjects. JAMA 310, 2191–2194.

Yamamoto, K., & Miura, K. (2012). Time dilation caused by static images with implied motion. *Experimental Brain Research*, *223*(2), 311–319. https://doi.org/10.1007/s00221-012-3259-5

Appendix

In our implementation of the UML procedure, the Cumulative Gaussian was selected as psychometric function (Donato et al., 2021):

$$p(correct) = \gamma + (1 - \gamma - \lambda)\frac{1}{2}\left[1 + erf\left(\frac{x - \alpha}{\sqrt{2\beta^2}}\right)\right] \quad \text{Eq. A1}$$

where α is the center of the psychometric function, *β* is associated with the slope, γ is the proportion correct for chance performance (i.e., 0.5), which set the lower bound of the psychometric function, and *λ* is the difference between the upper asymptote of the function and one, indicating the lapses rate.

The initial signal strength, i.e., number of coherently oriented dipoles, was set at 2000 dipoles, with limits in the interval [100 2000]. The range of the parameter α was in the interval [200 1900], with a prior uniform distribution. The range of the parameter *β* was in the interval [0.05 20] with a prior uniform distribution, and the range of the parameter *λ* was in the interval [0 0.1], again with a prior uniform distribution.

For each participant, the coherence threshold was calculated from the best parameters of the Cumulative Gaussian estimated with the UML procedure, finding the coherence corresponding to the 79% correct performance from the psychometric function.